# COMPARISON OF ELECTRODEPOSITION ASPECTS AND CHARACTERISTICS OF Ni-W AND Co-W ALLOY NANOCRYSTALLINE COATINGS

**Z. Ghaferi*, K. Raeissi, M. A. Golozar, A. Saatchi and S. Kabi**
* *ghaferi_z@yahoo.com*
**Received: August 2010** **Accepted: December 2010**

**Department of Materials Engineering, Isfahan University of Technology, Isfahan, Iran.**

***Abstract:*** *Ni-W and Co-W alloy nanocrystalline coatings were electrodeposited on copper substrate at different current densities. Electrochemical impedance spectroscopy (EIS) results showed that the codeposition mechanism of tungsten in Ni-W deposition is the reduction of tungsten oxide which changed to the reduction of tungsten-containing ion complexes at higher current densities. In Co-W electrodeposition, the tungsten codeposition takes place via reduction of tungsten oxide, although, the role of tungsten-containing complexes at higher current densities cannot be ruled out. The surface morphology of Ni-W coatings was crack-free and was strongly dependent on deposition current density. In addition, higher grain size and lower tungsten content were obtained by increasing the current density. In Co-W coatings, no obvious variation in surface morphology was observed except for the fine cracks appeared at higher current densities. In this system the grain size remained almost constant with increasing current density. The microhardness values of Ni-W and Co-W coatings decreased due to the increase in the grain size and/or decrease in tungsten content.*

***Keywords:*** *Co-W; Ni-W; electrodeposition; EIS; nanocrystalline; coating*

## 1. INTRODUCTION

Recently, the replacement of hard chromium coating with coatings that have good properties and non-polluting nature has gained increased attentions. One of more attractive candidate is iron-group alloys containing tungsten [1]. These alloys have outstanding tribological, mechanical, magnetic and electrical properties. Furthermore, they have good corrosion resistance in acidic and alkaline media [2, 3]. Tungsten-rich alloys show excellent wear resistance in applications such as valves, dies, cutting tools, gas turbines and jet engines [3]. These alloys can also be used as electrode for hydrogen evolution [2, 4]. Tungsten metal cannot be electrodeposited in pure state from aqueous electrolytes itself. But, it can be co-deposited with transition metals from aqueous solutions [5-9].

In order to improve the tribological and thermal stability of these coatings, there have been some efforts to increase tungsten content. One method is increasing the bath temperature to facilitate the tungsten transportation by increasing ion mobility and decreasing solution viscosity. However, with increasing the temperature up to 50 $^{o}$C, tungsten content decreases due to higher hydrogen evolution [1]. Another method is the decrease in citrate ion concentration. It is reported that the formation of ternary complexes containing (Ni/Co)-tungstat-citrate is necessary for tungsten deposition [10]. In the presence of excess citrate, the citrate can form complex with Co or Ni which is a path to deposition of these metal, and thus, the tungsten content of deposit decreases [6]. Some researchers believe that by increasing the current density, the tungsten content of deposit decreases which refers to higher hydrogen evolution [11]. By increasing the pH of electrolyte, the concentration of H+ decreases, so tungsten can deposit easier [12]. Dulal et al. [13] have reported that the morphology of Co-W-P coatings extremely depend on the pH of electrolyte.

Tungsten alloys usually deposits from sulfamate and ammoniacal citrate electrolyte [12]. Although citrate containing electrolytes are non-toxic, they cause the low current efficiency [8. 14]. In order to overcome this problem, ammonia is commonly added to improve the current efficiency. However, ammonia enhances only the transport of nickel/cobalt ions by complex formation and consequently reduces the tungsten in deposit [14].

The goal of this work is to study the electrochemical aspects of deposition in Ni-W

and Co-W coatings. The coating properties such as surface morphology, structure, tungsten content and hardness are also compared.

## 2. MATERIALS AND EXPERIMENTAL PROCEDURES

A disk of 0.85 $cm^2$ surface area of copper was used as substrate. The substrate was mechanically polished down to 600 grade abrasive paper and then electropolished in a solution containing 65% phosphoric acid and 35% distilled water for 15 min [15]. The deposition was performed at room temperature using a digital coulometer model BHP 2050. The coatings were electrodeposited using a platinum wire as the anode electrode. The composition of the baths is shown in Table 1. Using dilute NaOH or $H_2SO_4$, pH of the baths was adjusted at 7.5. The number of coulombs passed during the electrodeposition was kept constant at 36. This led to a theorical coating thickness of 13 $\mu$m. The real coating thickness was around 10$\mu$m measured by observing the cross section of coated specimens.

In order to measure the impedances, an EG&G AC responser (model 1025) coupled with an EG&G potentiostat/galvanostat (model 263A) was used. The voltage amplitude was 10 mV and the frequency range was 100 kHz -10 mHz. The tests were carried out in a standard cell with three-electrode system using platinum wire as auxiliary and saturated calomel electrode (SCE) as reference.

A Philips XL30 scanning electron microscope (SEM) was used to study the coating surface morphology. The presence of tungsten in the coatings was determined by energy dispersive spectroscope (EDS) coupled with SEM. The grain size of the coatings was determined from x-ray patterns obtained by diffractometer (Philips X'pert). The grain size was calculated using the angular width of the nickel (111) and cobalt (100) peaks at its full-width at half maximum (FWHM) in conjunction with the Scherrer equation (eq. 1) [16].

$$d = \frac{0.9\lambda}{\beta.\cos\theta} \quad (1)$$

Where $\lambda$, $\beta$ and $\theta$ are the wavelength of $CuK_\alpha$ (1.5406 °A), the integral width and the

**Table 1.** Composition of the baths and conditions of electrodeposition.

| Composition | Effect | Co-W bath ($g l^{-1}$) | Ni-W bath ($g l^{-1}$) |
|---|---|---|---|
| $CoSO_4.7H_2O$ | Co source | 40.24 | .... |
| $NiSO_4.6H_2O$ | Ni source | .... | 22.24 |
| $Na_3C_6H_5O_7.2H_2O$ | Complexing agent | 178.58 | 178.58 |
| $Na_2WO_4.2H_2O$ | W source | 51.22 | 51.22 |
| $NH_4Cl$ | Improves faradic efficiency | 26.74 | 26.74 |
| NaBr | Improves conductivity | 15.42 | 15.42 |
| Temperature | 298 K | | |
| pH | 7.5 | | |
| Current density | 2.5, 15 and 50 mA $cm^{-2}$ | | |

diffraction angle, respectively. The step size was 0.04 degree and the diffraction angles were 20-50 degree. The four-parameter Gaussian function was used for curve fitting required for FWHM determination. Instrumental line broadening was also measured by a silicon standard specimen and corrected by the Gaussian-Cauchy equation. The microhardness values were determined by Vickers technique at 5 g load applied for about 20 s, using a diamond pyramidal indenter in Leitz microhardness tester. The reported values are the average of four measurements.

## 3. RESULTS AND DISCUSSION

### 3. 1. Selection of Deposition Current Densities

Fig. 1 shows the cathodic scan readings drawn in Ni-W and Co-W electrodeposition baths at room temperature. The potential was swept between -0.25 and -2.1 V vs. SCE with scan rate of 40 mV $s^{-1}$. The suitable current densities for deposition were selected from these curves. For both readings, the current densities of 2.5 and 15 mA $cm^{-2}$ belong to the activation and mix polarization regions, respectively. The current density of 50 mA $cm^{-2}$ is related to diffusion region in Ni-W alloy deposition [17], but, again it belongs to mix region for Co-W alloy deposition. The steady state potentials corresponding to the above deposition current densities are estimated from galvanostatic plots shown in Fig. 2.

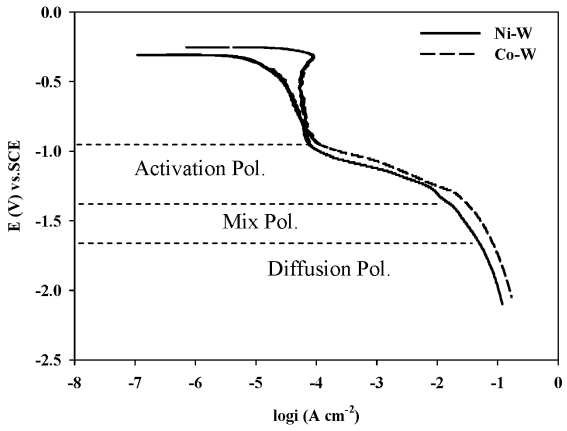


**Fig. 1.** Cathodic polarization plots of Ni-W and Co-W depositions obtained at room temperature (scan rate = 40 mV $s^{-1}$)

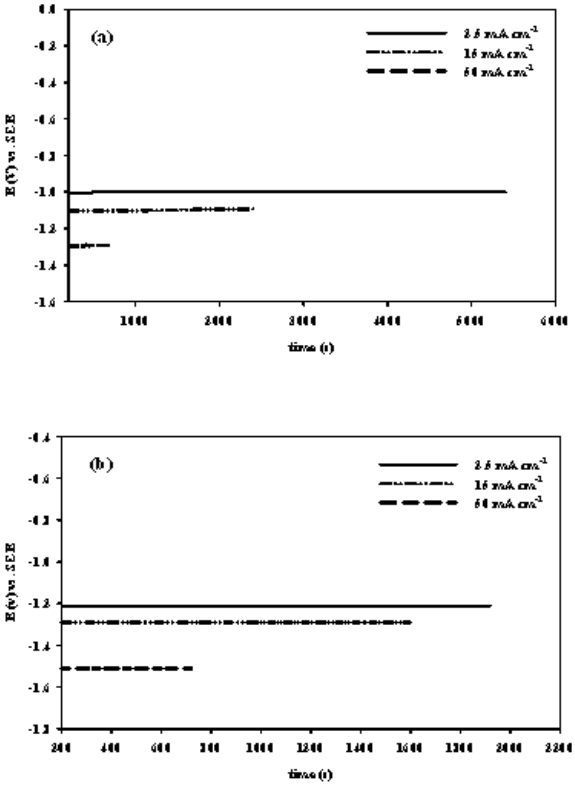


**Fig. 2.** Galvanostatic readings employed to obtain steady state potentials in (a) Co-W and (b) Ni-W alloy depositions.

### 3. 2. Morphological Observation

Fig. 3 shows the surface morphologies of Ni-W and Co-W alloy coatings deposited at current densities of 2.5, 15 and 50 mA $cm^{-2}$. Figs. 3(a-c) show the surface morphologies of Co-W electrodeposits. As seen, the amount of nodules and micro-crack densities are increased by increasing the deposition current density. Similar behaviour was observed by Santana et al. [18]. For Ni-W coating, a typical cauliflower surface morphology is obtained at 2.5 mA $cm^{-2}$ (Fig. 3d). Increasing the deposition current density resulted in semi-distorted cauliflower morphology at 15 mA $cm^{-2}$ (Fig. 3e). Further increase in current density to 50 mA $cm^{-2}$, resulted a nodular surface morphology as seen in Fig.3f. It is concluded that the surface morphology of Ni-W coatings depends strongly on deposition current density and varies significantly by entering into different polarization regions [17]. Some researchers believe that the Ni-W-Co alloys deposited on copper substrate present a substantial decrease in

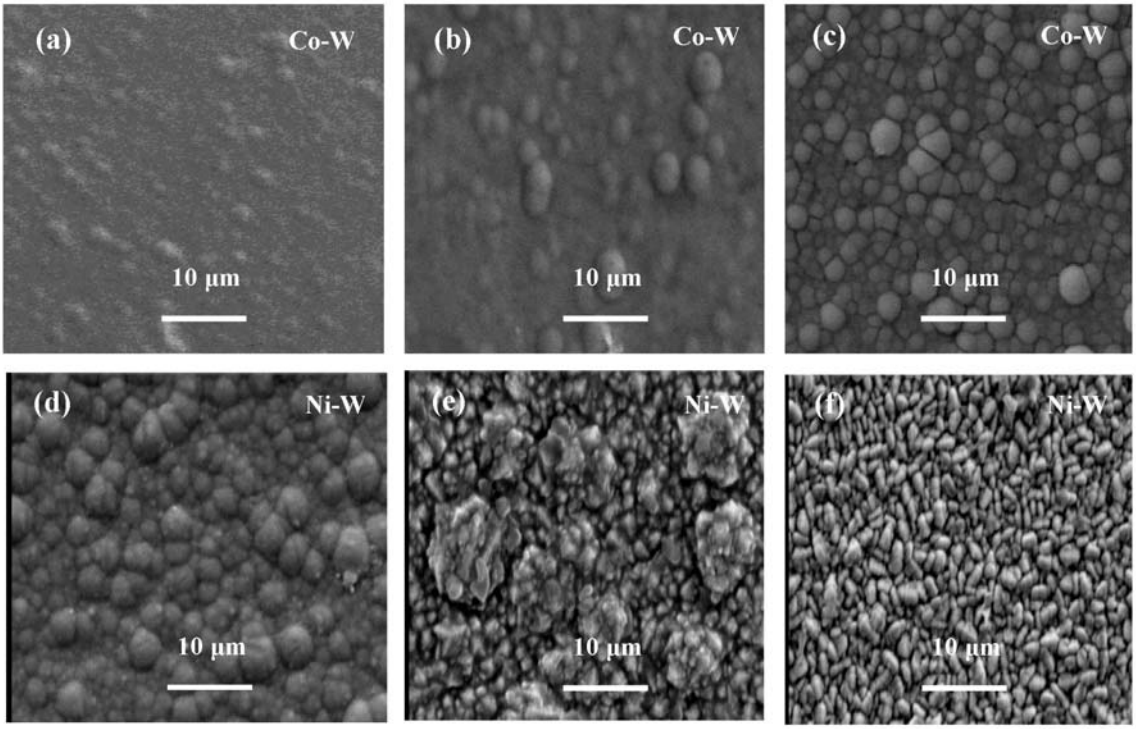


**Fig. 3.** SEM micrographs of the coatings deposited at: (a, d) 2.5 mA $cm^{-2}$, (b, e) 15 $mAcm^{-2}$ and (c, f) 50 $mAcm^{-2}$

the number of microcracks when compared to Co-W alloy deposits [2]. This is due to the presence of Ni in alloy and indicates that Ni and Ni-containing matrixes show more resistance against cracking compared to Co and Co-containing matrixes.

Mizushima et al. [19] have noticed that the microcracks are caused by the relaxation of internal tensile stresses. They suggested that the hydrogen ingression into the deposit occurs during the electrodeposition and its subsequent release creates a high tensile stress which can develop the microcracks in deposit. It is reported that the electrodepositing by pulse technique can reduce the stresses because hydrogen can diffuse out of the deposit during off-period of pulse plating [14]. However, Santana et al. [18] have reported that the microcracks can be created due to the internal stresses built up by the presence of tungsten in alloy. The absence of microcracks in Ni-W electrodeposits is also reported by Moussa et al. [12]. They attributed this to the relatively high cathodic current efficiency, and consequently, less hydrogen evolution during Ni-W deposition compared to other tungsten-containing alloy depositions.

### 3. 3. EIS Investigations

There are several hypotheses for tungsten codeposition with iron-group metals. In one theory, it proposes the existence of tungsten oxide and its subsequent reduction by the atomic hydrogen held on the freshly deposited iron-group metal (Holt's mechanism) [20]. Another idea for tungsten codeposition is the reduction of complex ions containing tungsten (Imanaga's mechanism) [20]. Some of these complexes are introduced as $[(M)(WO_4)_2(H)_2(Cit)]^{3-}$, $[(M)(WO_4)(Cit)(H)]^{2-}$ and $[M(HWO_4)(HCit)]^{2-}$, where M represents Co or Ni ions [6, 21].

In order to investigate the electrochemical aspects of electrodeposition, EIS tests were performed at corresponding potentials obtained for 2.5, 15 and 50 mA $cm^{-2}$, i.e. -1000, -1100 and -1300 mV for Co-W and -1200, -1300 and -1500 mV for Ni-W depositions. The Nyquist plots for both Ni-W and Co-W alloy systems obtained at the above potentials are shown in Fig. 4. As seen from Figs. 4a and d, there is a capacitive loop at very high frequencies at 2.5 mA $cm^{-2}$. This loop probably belongs to the formation of tungsten oxide film during the electrodeposition process [15]. The second

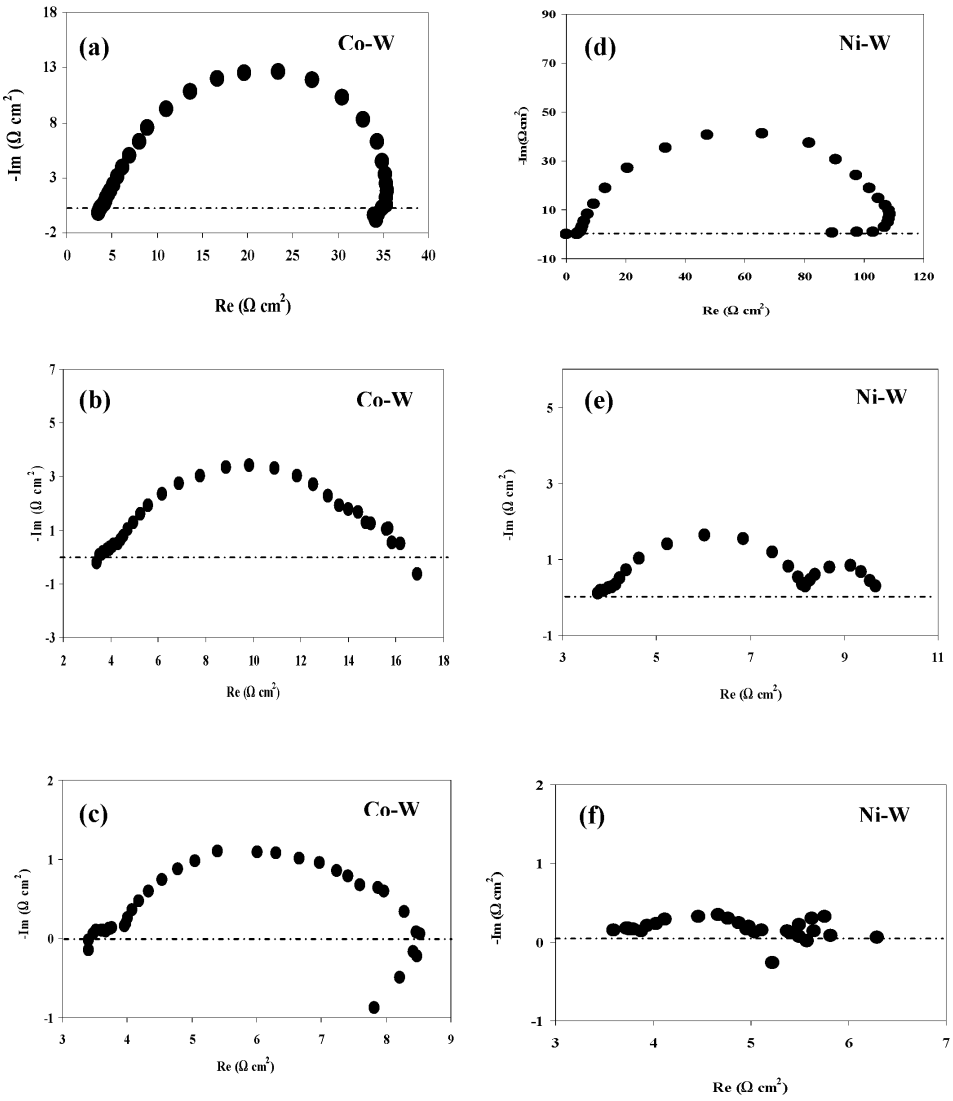


**Fig. 4.** Nyquist plots of the coatings at: (a, d) 2.5 mA $cm^{-2}$, (b, e) 15 mA $cm^{-2}$, (c, f) 50 mA $cm^{-2}$

**Table 2.** Data extracted from Nyquist plots in Fig. 4 for Co-W and Ni-W deposition.

| | Current density in Co-W deposition (mA $cm^{-2}$) | | | Current density in Ni-W deposition (mA $cm^{-2}$) | | |
|---|---|---|---|---|---|---|
| | 2.5 | 15 | 50 | 2.5 | 15 | 50 |
| E (mV) | -1000 | -1100 | -1300 | -1200 | -1300 | -1500 |
| $R_{ct}$ (Ω $cm^2$) | 31.5 | 8.2 | 3.5 | 128.7 | 5 | 2.2 |
| $CPE_{dl}$(μF $cm^{-2}$) | 780 | 550 | 570 | 376 | 164 | 106 |

capacitive loop at medium frequencies is related to double layer capacitance parallel to charge transfer

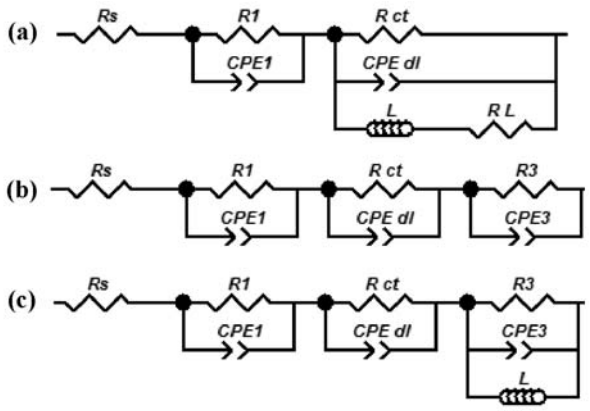


**Fig. 5.** Equivalent circuits estimated by ZVIEW program, (a) for Ni-W and Co-W coatings deposited at 2.5 mA $cm^{-2}$, (b) Ni-W coatings deposited at 15 and 50 mA $cm^{-2}$, (c) Co-W coatings deposited at 15 and 50 mA $cm^{-2}$, Where Rs is the uncompensated solution resistance, $R_1$ and $CPE_1$ are resistance and constant phase element of oxide layer, $R_{ct}$ and $CPE_{dl}$ are charge transfer resistance and double layer capacitance, $R_3$ and $CPE_3$ are resistance and constant phase element related to the diffusion of complexes, L is the inductor referred to the adsorption of hydrogen and $R_L$ is the resistance of the inductor.

resistance which is similar in shape for both Ni-W and Co-W depositions [15]. Finally, there is a small inductive loop at very low frequencies corresponding more likely to the adsorption of hydrogen [22, 23]. Kabi et al. [17] have reported these loops in the previous research. By decreasing the potential, a third capacitive loop is appeared just before the inductive loops in both Co-W and Ni-W electrodeposition systems as seen in Figs. 4b, c, e and f. However, the inductive loop is disappeared in Ni-W electrodeposition system (Figs. 4e, f). It is noticeable that the third capacitive loop observed as a distinct loop at low frequencies in Ni-W electrodeposition cannot be distinguished well in Co-W deposition and it is overlapped by the previous loop in Nyquist plots. It has been reported that this very low-frequency capacitive loop is related to slow bulk diffusion of electro-active complex ions such as those discussed above [15, 17, 22]. Juskenas et al. [24] have stated that the concentration of these complexes is generally very low, so it causes mass transport limitation in deposition process. It is assumed that the complex ions play an important role in W codeposition. As seen from Fig. 4f, by decreasing the cathodic potential, the third capacitive loop was scattered. This is due to the relaxation phenomena takes place in deposition process [15].

As mentioned, by increasing the current density, the very low-frequency inductive loop cannot be observed in Ni-W electrodeposition (Figs. 4e, f). However, this loop exists for Co-W deposition at higher current densities (Figs. 4b, c). This means that the Holt's mechanism is valid at all current densities in Co-W deposition, but, the role of Imanaga's mechanism at higher current densities cannot be ruled out. Table 2 shows the elements of electrical equivalent circuits extracted from Nyquist plots in Fig. 4 by simulation using ZVIEW program (Fig. 5). As seen, charge transfer resistance (Rct) is decreased with cathodic potential for both Ni-W and Co-W systems. This may be related to the increase in surface diffusion of adions which facilitates their flux toward the active growing sites [17, 25].

### 3. 4. Grain Size Determination and Tungsten Content

XRD patterns of as-deposited alloy coatings are shown in Fig. 6. From these patterns, solid solutions of fcc and hcp structures can be deduced for Ni-W and Co-W alloys, respectively. Although, electrodeposited alloys often exhibit the phases predictable from the equilibrium phase diagram, but there are some exceptions. It means that the phase structure of electrodeposited alloys may differ from that obtained by thermal equilibration [26, 27]. For example, it is reported that Co-25%W coating prepared by electrodeposition is a single phase solid solution, while, a double phase structure is predicted from

**Table 3.** Tungsten content and grain size of Co-W and Ni-W coatings obtained from x-ray patterns and EDS analysis

| | Current density in Co-W deposition($mA\ cm^{-2}$) | | | Current density in Ni-W deposition($mA\ cm^{-2}$) | | |
|---|---|---|---|---|---|---|
| | 2.5 | 15 | 50 | 2.5 | 15 | 50 |
| W content (at. %) | 16 | 12 | 12 | 18 | 8 | 5 |
| Grain size (nm) | 19 | 18 | 18 | 13 | 18 | 22 |

the equilibrium phase diagram [26, 28].

Table 3 shows the average grain size and tungsten content of coatings obtained at different current densities. As mentioned before, increasing the deposition current density resulted in mass transport limitation for W codeposition which decreased the tungsten content in deposited alloys. According to Krolikowski et al. [29], grain refinement in Ni-W coatings is

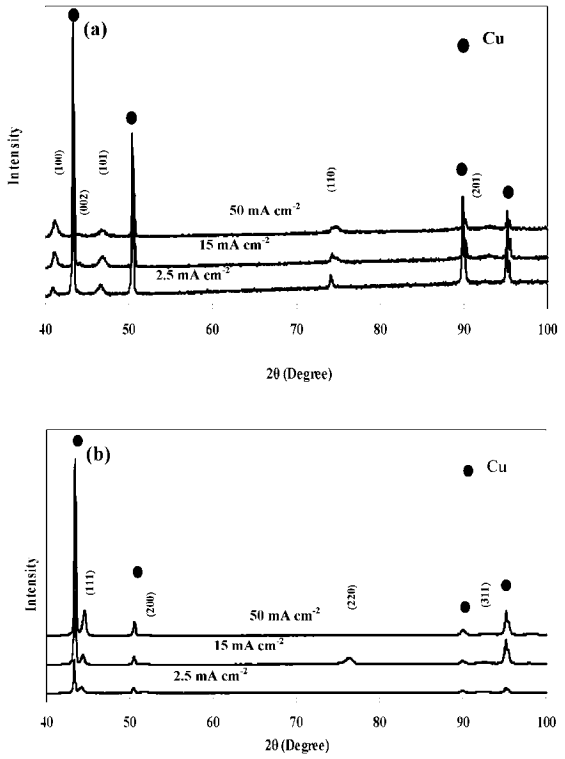


**Fig. 6.** XRD patterns corresponding to: (a) Co-W and (b) Ni-W coatings

achieved by increasing the tungsten content. As seen in Table 3, increasing the deposition current density decreases the tungsten content in Ni-W deposited coatings and increases the grain size [17]. These results are in good agreements with Krolikowskis observation. However, the grain size in Co-W alloy coatings remains almost constant with variation of current density.

### 3. 5. Microhardness Measurement

Fig. 7 shows microhardness value and its variation for both Ni-W and Co-W alloy coatings obtained at different current densities. The highest microhardness magnitudes are obtained for the coatings with the highest tungsten content deposited at 2.5 mA $cm^{-2}$. It is reported that the microhardness of alloys increases by solid solution hardening or decrease in grain size [30]. As is seen in Table 3, by increasing the current density, the tungsten content of Ni-W alloy coatings is decreased and the grain size is increased. It seems that the improved microhardness found in Ni-W alloy coating deposited at low deposition current density should be due to the simultaneous effects of decrease in grain size and increase in tungsten content. However, Schuh et al. [30] believe that the role of solid solution hardening in Ni-W nanocrystalline alloys (i.e. the effect of W element) is negligible compared with the very strong effect of grain refining. Eliaz et al. [11] reported that the hardness of as-deposited Ni-W alloys is typically in the range of 450-768 HV, which confirms the results obtained in this study.

According to Table 3, no remarkable variation

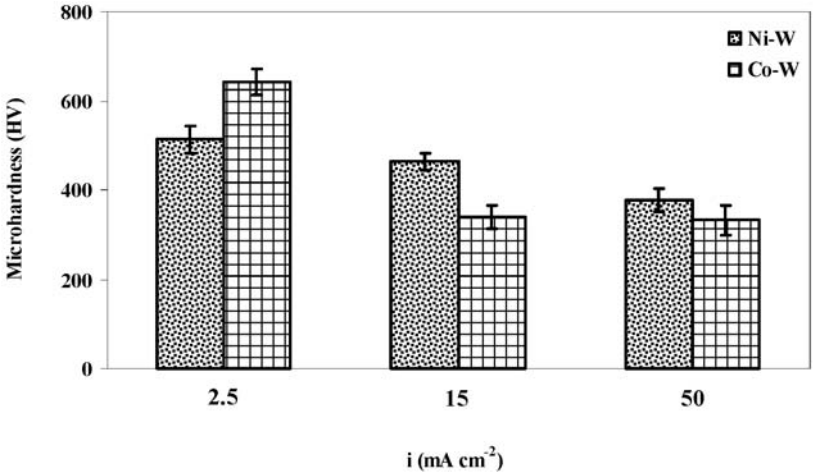


**Fig. 7.** Microhardness values for Ni-W and Co-W coatings.

is observed in grain size of Co-W coatings with current density. However, the hardness of Co-W coatings decreases by increasing current density and this may be due to lower tungsten content obtained. Capel et al. [31] reported that the surface hardness of Co-30wt%W alloy (almost near 12 at%W) which has similar tungsten content shows a value around 450 HV.

## 4. CONCLUSIONS

1. Although the surface morphology of Ni-W coatings was crack-free and strongly dependent on deposition current density, but the surface morphology of Co-W coatings showed no obvious variation with deposition current density except for the fine cracks appeared at higher current densities. This means that the Co alloy coatings are more prone to cracking than Ni alloy coatings.
2. Codeposition of tungsten in both Ni-W and Co-W systems occurs through reduction of tungsten oxide and tends to the redaction of tungsten ion complexes by increasing the current density.
3. The microhardness of Ni-W or Co-W coatings decreases due to the increase in grain size and decrease in tungsten content. For this reason, the highest microhardness value is obtained at 2.5 mA $cm^{-2}$.

## REFERENCES

1. Abdel Hamid Z., Electrodeposition of cobalt-tungsten alloys from acidic bath containing cationic surfactants, Mater. Lett. 2003, 57, 2558-2564.
2. Santana R.A.C, Campos A.R.N., Medeiros E.A., Oliveira A.L.M., Silva L.M.F., Prasad S., Studies on electrodeposition and corrosion behaviour of a Ni-W-Co amorphous alloy, J. Mater. Sci. 2007, 42, 9137-9144.
3. Mayanna S. M., Ramesh L., Maruthi B. N., Landolt D., AES investigation of electrochemically deposited Co-W layers on copper, J. Mater. Sci. Lett. 1997, 16, 1305-1306.
4. Ma M., Donepudi V. S., Sandi G., Sun Y. K., Prakash J., Electrodeposition of nano-stractured nickel-21% tungsten alloy and evaluation of oxygen reduction reaction in a 1% sodium hydroxide solution, Electrochim. Acta, 2004, 49, 4411-4416.
5. Svensson M., Wahlstrom U., Holmbom G., Compositionally modulated cobalt-tungsten alloys deposited from a single ammoniacal electrolyte, Surf. Coat. Technol. 1998, 105, 218-223.
6. Younes-Metzler O., Zhu L., Gileadi E., The anomalous codeposition of tungsten in the presence of nickel, Electrochim. Acta, 2003, 48, 2551-2562.
7. Galikova Z., Chovancova M., Danielik V., Properties of Ni-W alloy coatings on steel substrate, Chem. Pap. 2006, 50, 353-359.
8. Ibrahim M. A. M., Abd el rehim S. S., Moussa S. O., Electrodeposition of nanocrystalline

cobalt-tungsten alloys from citrate electrolytes,J. Appl. Electrochem. 2003, 33, 627-633.
9. Dulal S.M. S. I., Kim T. H., Shin C. B., Kim C. -K., Electrodeposition of CoWP film, IV. Effect of applied potential and current density, J. Alloys Comp. 2008, 461, 382-388.
10. Younes O., Zhu L., Rosenberg Y., Shacham-Diamand Y., Gileadi E., Electroplating of amorphous thin films of tungsten/nickel alloys, Langmuir, 2001, 17, 8270-8275.
11. Eliaz N., Sridhar T. M., Gileadi E., Synthesis and characterization of nickel tungsten alloys by electrodeposition, Electrochim. Acta, 2005, 50, 2893-2904.
12. Moussa S. O., Ibrahim M. A. M., Abd el rehim S.S., Induced electrodeposition of tungsten with nickel from acidic citrate electrolyte, J. Appl. Electrochem. 2006, 36, 333-338.
13. Dulal S. M. S. I., Yun H. J., Shin C. B., Kim C. -K., Electrodeposition of CoWP film V. structural and morphological characterization, Appl. Surf. Sci. 2009, 255, 5795-5801.
14. Mizushima I., Tang P. T., Hansen H. N., Somers M. A. J., Residual stress in Ni-W electrodeposits, Electrochim. Acta, 2006, 51, 6128-6134.
15. Farzaneh M. A., Raeissi K., Golozar M. A., Effect of current density on deposition process and properties of nanocrystalline Ni-Co-W alloy coatings, J. Alloys Comp. 2010, 489, 488-492.
16. Cullity B. D., Stock S. R., Elements of x-ray diffraction, Addision-Wesley, London, 2001.
17. Kabi S., Raeissi K., Saatchi A., Effect of polarization type on properties of Ni-W nanocrystalline electrodeposits, J. Appl. Electrochem. 2009, 39, 1279-1285.
18. Santana R. A. C., Prasad S., Campos A. R. N., Araujo F.O., Da Silva G.P., De Lima-Neto P., Electrodeposition and corrosion behaviour of a Ni-W-B amorphous alloy, J. Appl. Electrochem. 2006, 36, 105-113.
19. Mizushima I., Tang P. T., Hansen N. H., Somers M. A. J., Development of a new electroplating process for Ni-W alloy deposits, Electrochim. Acta, 2005, 51, 888-896.
20. Akiyama T., Fukushima H., Recent study on the mechanism of the electrodeposition of iron-group metal alloys, ISIJ International, 1992, 32, 787-798.
21. Obradovic M. D., Stevanovic R. M., Despic A.R., Electrochemical deposition of Ni-W alloys from ammonia-citrate electrolyte, J. Electroanal. Chem. 2003, 552, 185-196.
22. Holm M., Okeefe T. J., Evaluation of nickel dposition by electrochemical impedancespectroscopy, J. Appl. Electrochem. 2000, 30, 1125-1132.
23. Sanaty-Zadeh A., Raeissi K., Saidi A., Properties of nanocrystalline iron-nickel alloys fabricated by galvano-static electrodeposition, J. Alloys Comp. 2009, 485, 402-407.
24. Juskenas R., Valsiunas I., Pakstas V., Selskis A., Jasulaitiene V., Karpaviciene V., Kapocius V., XRD, XPS and AFM studies of the unknown phase formed on the surface during electrodeposition of Ni-W alloy, Appl. Surf. Sci. 2006, 253, 1435-1442.
25. Hassani Sh., Raeissi K., Golozar M. A., Effect of saccharin on the electrodeposition of Ni-Co nanocrystalline coatings, J. Appl. Electrochem. 2008, 38, 689-694.
26. Lowenheim F. A., Modern electroplating, John Wiley & Sons, New York, 1973.
27. Obradovic M. D., Bosnjakov G. Z., Stevanovic R.M., Maksimovic M.D., Despic A.R., Pulse and direct current plating of Ni-W alloys from ammonia-citrate electrolyte, Sur. Coat. Technol. 2006, 200, 4201-4207.
28. ASM Handbook, Vol. 3, Alloy phase diagrams The Materials Information Society, ASM International, Materials Park OH, 1992.
29. Krolikowski A., Plonska E., Ostrowski A., Donten M., Stojek Z., Effect of compositional and structural features on corrosion behavior of nickel-tungsten alloys, J. Solid State Electrochem. 2009, 13, 263-275.
30. Schuh C. A., Nieh T. G., Iwasaki H., The effect of solid solution W additions on the mechanical properties of nanocrystalline Ni, Acta Mater. 2003, 51, 431-443.
31. Capel H., Shipway P. H., Harris S. J., Sliding wear behaviour of electrodeposited cobalt-tungsten and cobalt-tungsten-iron alloys, Wear, 2003, 255, 917-923.